공학석사 학위논문

Low Temperature Crystalized $LiNi_{0.5}Mn_{1.5}O_4$ Cathode Thin Films by Excimer Laser for Flexible Thin Film Batteries

엑시머 레이저로 저온 소결된 $LiNi_{0.5}Mn_{1.5}O_4$ 양극 박막을 이용한 유연 박막 전지

2014년 6월

서울대학교 대학원

공과대학 화학생물공학부

Yim Haena

Low Temperature Crystalized $LiNi_{0.5}Mn_{1.5}O_4$ Cathode Thin Films by Excimer Laser for Flexible Thin Film Batteries

지도 교수 성 영 은

이 논문을 공학석사 학위논문으로 제출함

2014 년 6 월

서울대학교 대학원

공과대학 화학생물공학부

Yim Haena

Yim Haena의 석사 학위논문을 인준함

2014 년 6 월

위 원 장	김대형	(인)
부위원장	성영은	(인)
위 원	최지원	(인)

Abstract

Low Temperature Crystalized $LiNi_{0.5}Mn_{1.5}O_4$ Cathode Thin Films by Excimer Laser for Flexible Thin Film Batteries

Yim Haena

School of Chemical & Biological Engineering

Seoul National University

The requirement of flexible and stretchable all-solid-state thin film lithium batteries have been steady increased as rapid development of flexible electronic devices such as smart cards, bio sensors, and roll-up displays. In order to satisfy the requirements, using the conventional polymer substrate is necessary for inexpensive and light weight battery. However, the cathode thin film, which is a critical component of thin film battery, certainly needs to be crystallized by high temperature annealing process because of the hindrance of solid-state lithium diffusion from any imperfections in the crystal. Eventually, the polymer substrate goes through sudden changes because of its poor resistance to high temperature, so a new direction

of crystallization should be considered.

Here, we demonstrated all-solid-state flexible thin film lithium battery using $LiNi_{0.5}Mn_{1.5}O_4$ cathode thin film, LIPON electrolyte, and Li metal anode thin film on polyimide (PI) substrate. The deposited cathode thin films were crystallized by the excimer laser annealing instead of high temperature annealing, so that the PI substrate was not damaged. Structural properties of the thin films were investigated by X-ray diffraction (XRD) and scanning electron microscopy (SEM). The electrochemical properties were measured using WBC3000 battery cycler and impedance analyzer. The results of this study shows the applicability of well-crystallized cathode film at low temperature, and it will be an important method in flexible devices.

Keywords: Flexible lithium thin film batteries, $LiNi_{0.5}Mn_{1.5}O_4$, Excimer laser annealing**,** sputtering

Student Number: 2012-23980

Contents

List of Figures

Chapter 1. Introduction

The steady reduction in size of electronic devices leads to the development of small-sized power sources. Moreover, because of the fast advance in the development of flexible electronics devices, such as flexible display[1], implantable medical devices[2], memory devices[3], micro-robot vehicles[4], and electronic skin patch[5], there is a huge need for further improvements in their power sources to make them possible to embed in flexible substrate. One of the solutions is using flexible all-solid-state lithium batteries which can decrease safety problem, liquid leakage during the bending state, and electrolyte deposition at high voltage through using solid electrolyte. Also, it can be easily integrated and packaged into micro-devices. Therefore, all-solid-state lithium thin film batteries are a great promising system for flexible power sources due to its safety, high operating voltage, and high energy density.

However, conventional fabrication processes are not appropriate to obtain flexible thin film batteries because the cathode and anode thin films required high annealing temperature to be crystallized, and this

high temperature affects flexible substrate like polymer, ultra-thin glass, and paper type substrate.

Because of this limitation, many techniques have been reported such as transfer method, new structured batteries, and intense pulsed laser annealing. For example, Y. H. Kwon et al. reported cable-type flexible lithium ion batteries which can achieve great mechanical flexibility. The basic design of cable-type batteries is composed of anode coiled into a hollow spiral core, cathode, called Al-Wire, surrounding anode, and packaging insulator[6]. Each component was electrodeposited on a Cu wire in regular sequence. Also, M. Koo et al. reported bendable inorganic thin film battery using the universal transfer approach, which enables to fabricate crystallized cathode thin film on polymer substrate[7]. The $LiCoO_2$ cathode thin film was annealed on the mica substrate and physically delaminated into thin sheet using sticky tape, and then transferred onto a PDMS polymer substrate. The bendable thin film batteries showed an operating voltage of 4 V and 106 $\mu Ah/cm^2$ at 5 μm cathode thin film.

However, these techniques are not congruous to large-scale and low-cost production because of complicate fabrication process. Therefore, we have demonstrated a fully flexible lithium thin film batteries on

polyimide substrate by excimer laser annealing which can crystallize cathode thin film in low temperature. Furthermore, we discuss the structural and electrochemical characteristics of the flexible lithium thin film batteries.

Chapter 2. Background

2.1 All-solid-state lithium thin film batteries

2.1.1 Overview

As a power source of various types of microchips, low-power medical applications, micro-scale energy storage system, all-solid-state lithium thin film batteries (TFBs) have been widely investigated as a power source. A schematic diagram of all-solid-state lithium thin film battery is presented in Fig. 1. As shown Fig. 1, TFBs consist of various component including current collectors, cathode, electrolyte, and anode thin films. The electrolyte separates ionic transport and electronic transport, so it determines the power density, the current density, and the safety of the batteries[8]. The cell potential is determined by the chemical potential difference of cathode and anode. Therefore, cathode material with high potential and anode material with low potential are required including high capacity property[9]. All thin films are deposited by various methods such as magnetron sputtering, thermal evaporator, and pulsed laser deposition.

TFBs provide the following benefits in general; TFBs are easily embedded in micro-devices because the thickness of fully packaged

TFBs is less than 1 mm; TFBs have long shelf lives with great cycleability up to thousands times; TFBs provide stable operating properties by using solid-state electrolyte; TFBs can be fabricated in various shape and any size; and TFBs provide high safety[10] and reliability[9].

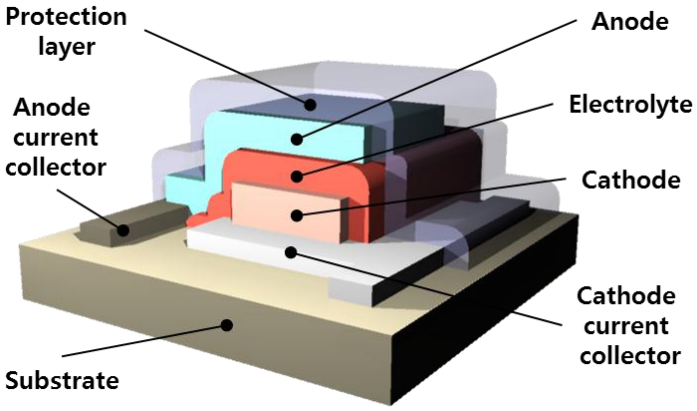

Fig. 2.1 schematic diagram of all-solid-state thin film battery

2.1.2 Operating principle

All-solid-state thin film batteries entail a reversible intercalation/de-intercalation of lithium ions during discharge/charge process like general lithium ion batteries[11]. During charge process, the positive material such as $LiCoO_2$ and $LiMn_2O_4$ is oxidized, and lithium ions are de-intercalated from the host matrix of positive material into the negative material. At that time, the negative material such as lithium metal and carbon is reduced. On the contrary, the positive material is reduced and negative material is oxidized during discharge process, and the reverse process is present as shown in Fig. 2.

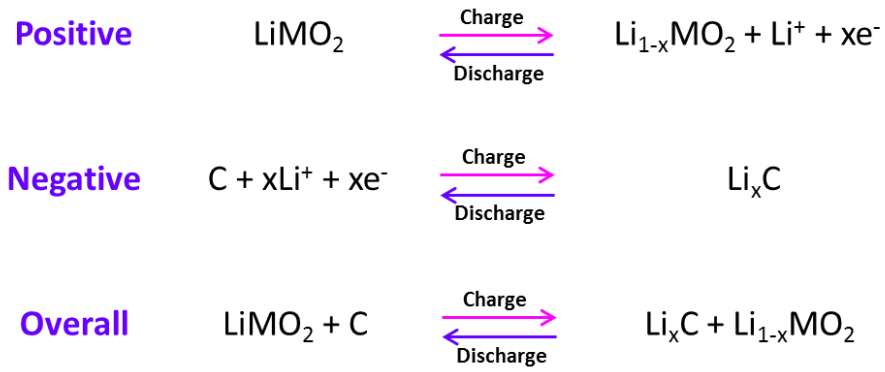

Fig. 2.2 electrochemical reactions during charge/discharge process

2.2 Components of lithium thin film batteries

2.2.1 Cathode thin films

Cathode thin films should be able to insert/de-insert lithium ions repeatedly and rapidly. Intensive research for cathode materials has led to the development several successful lithium insertion compounds. In consequence of the research, transition metal oxides based on layered, spinel, and olivine structure have been widely used in the past decades.

The first commercialized cathode material is $LiCoO_2$, which has layered structure, because of its advantages like easy fabrication, high theoretical capacity, fast lithium intercalation, and good cyclability. However, only half of the lithium ions can be intercalated for reversible operation and safety issues with its toxicity has created the effort to develop alternative materials.

Spinel structure $LiMn_2O_4$ is currently commercialized due to its high rate performance, high energy density, low cost, and low toxicity. However, only 80 percent of the lithium can be reversibly extracted and it limits the discharge capacity. Also, the operating potential of $LiMn_2O_4$ versus Li/Li^+ is only 3.5 V, and capacity fade is frequently appeared because of the collapsed spinel structure caused by the Jahn-

Teller effect.

In order to overcome these limitations, other transition metal substitute for Mn in $LiMn_2O_4$ has been studied recently such as Sn, Cr, Ni, Fe, and Co[12]. Among others, $LiNi_{0.5}Mn_{1.5}O_4$ is considered as remarkable cathode material because of its high operating voltage of 4.7 V with the theoretical capacity of 146.6 mAh/g, good cyclability, and high power density.

2.2.2 Electrolyte

Lithium ion conducting solid-state electrolyte should provide the high lithium ion conductivity without electronic conductivity, wide potential window at cathode and anode electrode, low cost, and environmentally friendly. Several electrolytes were reported which fulfill these conditions. At the beginning of the research, Li_3N and Li-βAl_2O_3 were reported, which showed great ionic conductivity of 10^{-3} Scm-1. However, they could not use as solid electrolyte because of their chemical instability. Since the late 1970s, crystalline oxide-based solid-state electrolytes have been explored such as Li_4GeO_4-Li_3VO_4 and $Li_{3x}La_{(2/3)-x}TiO_3$. However, these electrolytes are shown great ion conductivity with well-ordered crystalline structure, which can be obtained after high temperature annealing. Therefore, these electrolytes are difficult to fabricate on polymer substrate for flexible batteries.

Lithium phosphorus oxinitride (LiPON) electrolyte has widely used because of its exceptional electrochemical stability against lithium metal and acceptable Li^+ ion conductivity even fabricated at room temperature. LiPON electrolyte thin film is generally prepared to 1 μm thin film by RF magnetron sputtering method, which is easily

form amorphous, dense, and free of grain boundaries film.

2.3 Deposition method

2.3.1 Magnetron sputtering system

Magnetron sputtering technique has widely used in various industrial depositions such as corrosion resistant coating, decorative coating, and thin film coating for optical or electrical properties. Basically, a target surface is bombarded by plasma ions and sputtering material is ejected on to the substrate as a thin film. The inert gas such as argon, which is filled in the vacuum chamber, creates a glow discharge and accelerates free electrons by applying a high voltage. These accelerated ions eject materials of sputtering target, and ejected materials are coated on substrate (Fig. 3).

Depend on the target material, DC or RF sputtering should be chose. DC sputtering, which operated by a constant voltage to accelerate the ions, can be used for a conducting target material because charges on the surface as the ions strike can move freely. On the other hand, RF sputtering can be used for an insulating target material in order to prevent charge remaining during the sputtering. DC magnetron sputtering uses a direct electron current and RF magnetron sputtering uses radio wave, so RF magnetron sputtering system is required much more volts above 10^{12} volts while DC magnetron sputtering is

required 5000 volts. Also, DC sputtering is required high pressure to achieve plasma, and RF sputtering can be operated at low pressure.

Compare with evaporation, magnetron sputtering used high energy atoms and formation smaller grain size with many grain orientations. Also, it provides the better adhesion between substrate and thin film, but the deposition rate is lower than evaporation.

2.3.2 Thermal evaporator

Thermal evaporation is one of the simplest physical vapor deposition techniques. A solid material is heated and the particles are deposited on the substrate.

The material to be deposited is located into a crucible, which is resistively heated by applying current. After enough temperature is given, the material is melted and remained stable vapor state. Then, the vapor atoms travel in straight lines and deposited on substrate as a thin film. Thermal evaporation is generally run in a high vacuum environment about 10^{-5} or 10^{-6} Torr in order to avoid reaction between the vapor and atmosphere gases, so high purity thin film can be achieved. Moreover, the deposition rate of thermal evaporation is generally higher than other thin film deposition methods, and the substrate is not damaged during deposition.

2.4 Excimer laser annealing(ELA)

Excimer laser annealing (ELA) is a technique for annealing materials without damage to thermally-weak substrate in rapid time, and it is the most common technology for fabricating polycrystalline silicon thin-film transistors (TFTs) for flat panel displays, mobile phone, and organic light emitting diode displays. The annealing is performed by irradiation with laser pulses from excimer laser source and transformed to the heat energy at surface of the sample, these transformed heat energy is diffused to the inside of thin film. The crystallinity and agrain size of sample are significantly affected by the irradiation conditions. Excimer laser annealing is much faster in contrast with conventional annealing process because of the very short pulse width of the excimer laser, so that is useful technique for the fabricate flexible thin film without thermal damage of substrate.

The key element of the exicmer laser annealing device is a beam forming and homogenizer. To improve the quality of laser and get homogeneous laser beam, a beam homogenizer was developed. The beam is focused down and across the beam scanner by dielectric mirrors.

By using excimer laser annealing, A . Pecora et al. reported low-

temperature fabricate polysilicon thin film transistor on polymer substrate[13], and the devices exhibit great field effect mobility up to 50 cm^2/Vs. Also, W. Chung et al. reported room temperature annealed indium tin oxide using XeCl excimer laser annealing for flexible display. The crystallinity of thin film was improved, and it brings better sheet resistance with great transmittance[14]. However, there is no report about ELA on all-solid-state lithium thin film batteries so far.

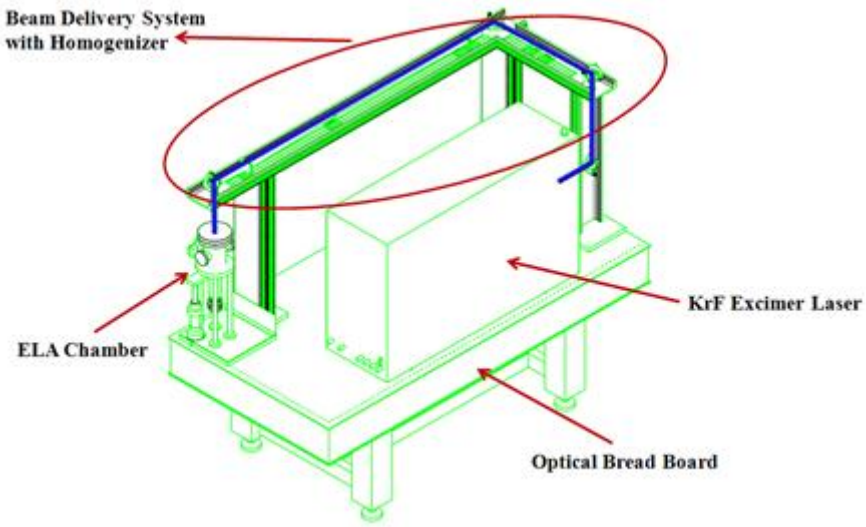

Fig. 2.3 Schematic diagram of eximer laser annealing system

Chapter 3. Experimental

3.1 Fabrication process

3.1.1 Current collector

Flexible all-solid-state thin film batteries were prepared on a 1.7 cm x 2.0 cm polyimide substrates. The polyimide substrates were cleaned by acetone and ethanol, and then rinsed in deionized water. Firstly, a 100 nm thick layer of Si_3N_4 and 300 nm thick layer of SiO_2 were deposited by PECVD system. The Si_3N_4 and SiO_2 films were used with the purpose of anti-thermal shock layer and anti-thermal diffusion layer. Following Si_3N_4 and SiO_2 deposition, 25 nm Ti "wetting" layer was DC-sputter deposited onto the polyimide substrate followed by 50 nm Pt layer. The base pressure of the chamber for DC-sputtering was lower than 5×10^{-6} Torr. The standard conditions used for deposition are as follows: working gas of argon, the Ar flow rate of 20 sccm, DC power of 30W, and total pressure of 3×10^{-3} Torr.

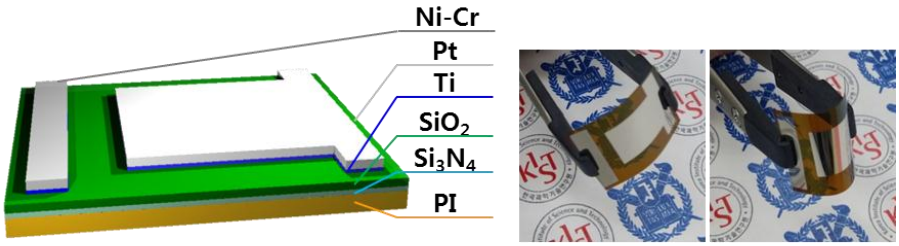

Fig. 3.1 Schematic diagram and photo-image of substrate structure

3.1.2 $LiNi_{0.5}Mn_{1.5}O_4$ cathode

3.1.2.1. Fabrication of $LiNi_{0.5}Mn_{1.5}O_4$ cathode thin film

$LiNi_{0.5}Mn_{1.5}O_4$ cathode thin films were deposited by on-axis RF magnetron sputtering on Pt/Ti/SiO_2/Si_3N_4/PI substrate with active area of 0.5 x 0.5 cm^2 using a 10 mTorr working pressure, 30 W RF power, and 30 sccm of Ar and 10 sccm O_2 flow rates at room temperature. The deposition chamber was evacuated by rotary pump and turbo-molecular pump. The base pressure of the sputtering chamber was controlled lower than $5x10^{-6}$ Torr, and the distance between target and substrate was fixed to 5 cm. Before deposition of cathode thin film, pre-sputtering was carried out for 15 min with the purpose of removing contaminant of target surface.

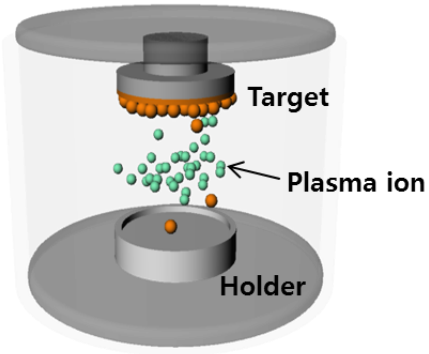

Process parameter	Condition
Target/sub.distance	5 cm.
Gas flow rate	Ar : O_2 = 30 : 10 sccm
Working pressure	10 mTorr
RF power	50 W
Deposition time	2 h
Deposition temp.	R. T.

Fig. 3.2 Schematic diagram of on-axis RF sputtering and sputtering condition

3.1.2.2. Excimer laser annealing of $LiNi_{0.5}Mn_{1.5}O_4$ cathode thin film

Deposited $LiNi_{0.5}Mn_{1.5}O_4$ cathode thin films were crystallized by Excimer laser annealing, which was carried out using KrF excimer laser p roviding excitation wavelength of 248 nm, without heating the polymer substrate. The beam homogenizing system was used and leads to the homogeneous beam shape of Gaussian fit. The ELA process was carried out by irradiation from the top surface of $LiNi_{0.5}Mn_{1.5}O_4$ cathode thin films, and a spot size of pulse was 5 mm × 5 mm. The repetition rate of pulses was 20 Hz, and the operating temperature was fixed at 200 ^{o}C. The total number of pulses was chosen in various ranges, and excimer laser energies of 40 mJ/cm^2 to 80 mJ/cm^2 were employed to obtain successfully annealed cathode thin films. The schematic of laser annealing system was shown in Fig.

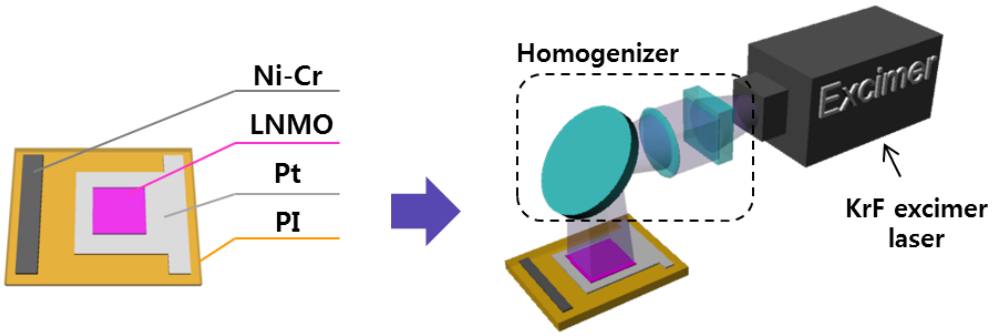

Fig. 3.3 Schematic diagram of cathode/current collector deposited substrate and laser annealing system

3.1.3 LiPON electrolyte

An amorphous lithium phosphorous oxynitride electrolyte thin film, which is well known as LiPON, were deposited by RF magnetron sputtering system with Li_3PO_4 2 inch target. The following deposition conditions were used for best ionic conductivity: RF power density of 40 W, N_2 flow of 40 sccm, working pressure of 10 mTorr, and the target to substrate distance of 7 cm. A base vacuum of 5×10^{-6} Torr was attained by a rotary pump and turbo molecular pump.

3.1.4 Li metal anode

Li metal anode thin film was easily deposited by a thermal evaporator method in the Ar filled glove box. High purity Li foil was used as an evaporation source, and it was placed in a molybdenum boat located inside a thermal evaporator. Deposition was performed when the base vacuum of 5 x 10^{-6} Torr was attained by a rotary pump and diffusion pump. Li metal thin films were deposited on substrates held at a pressure less than 2x10-^{5} Pa, and a deposition current range was controlled below 120 A.

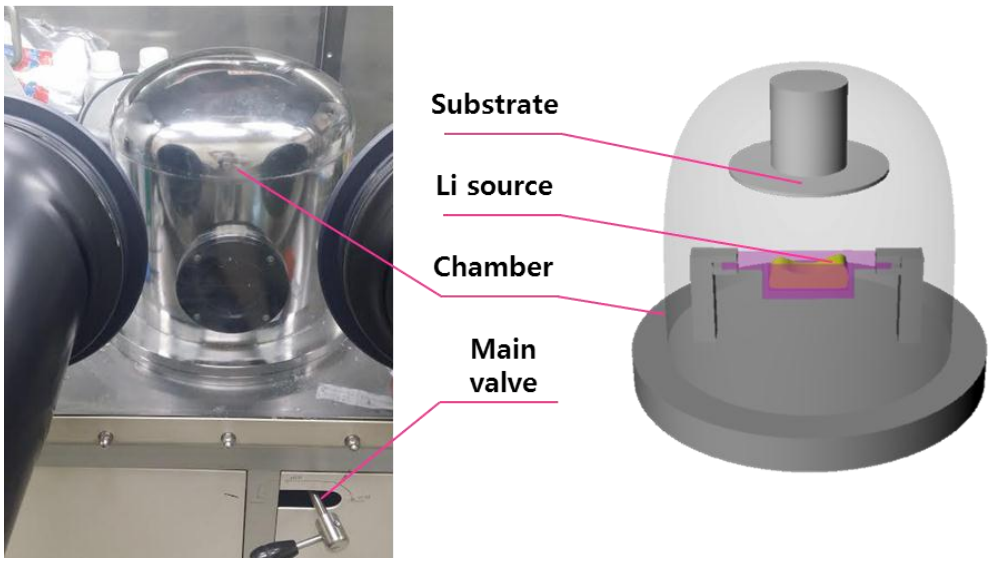

Fig. 3.4 A photo image and schematic diagram of the lithium thermal evaporator

3.2 Properties

3.2.1 Structural properties

The phase identification of the thin film was carried out with an X-ray diffractometer (XRD) (D/Max-2500 (Rigaku, USA), using Cu Kα radiation. The size and morphology of the thin films were characterized using a field emission scanning electron microscope (FESEM) operated at 10 kV. Before investigating images, the thin films were coated with a thin Pt layer to reduce surface charging effects. Auger electron spectroscopy (AES) depth profiling analysis was performed to analysis the element distribution through thickness by a scanning Auger nanoprobe PHI-700 model. For the AES analysis, an electron beam of 10 keV was irradiated on the sample surface.

3.2.2. Electrochemical properties

The AC impedance was measured from electrode/LiPON/electrode sandwich structures (Fig.) in order to obtain ionic conductivity of the LiPON thin films. The Pt bottom electrode was deposited on Si substrate, and the LiPON thin film was deposited with thickness of 1 μm. After that, Pt top electrode was deposited to an area of 0.7 x 0.5 mm. The AC impedance measurements were performed at room temperature at frequencies from 100 Hz to 100 MHz.

Electrochemical measurement were performed using WBCS3000 (WonATech, South Korea) in an argon filled glove box. For preparing the positive electrode, $LiNi_{0.5}Mn_{1.5}O_4$ cathode thin film was deposited on $Pt/Ti/SiO_2/Si_3N_4/PI$ substrate and annealed by excimer laser annealing. LiPON thin film was used for solid-state electrolyte and pure Li metal was used as a negative electrode. The cells were galvanostatically charged and discharged from 3.5 V to 4.9 V at various current densities.

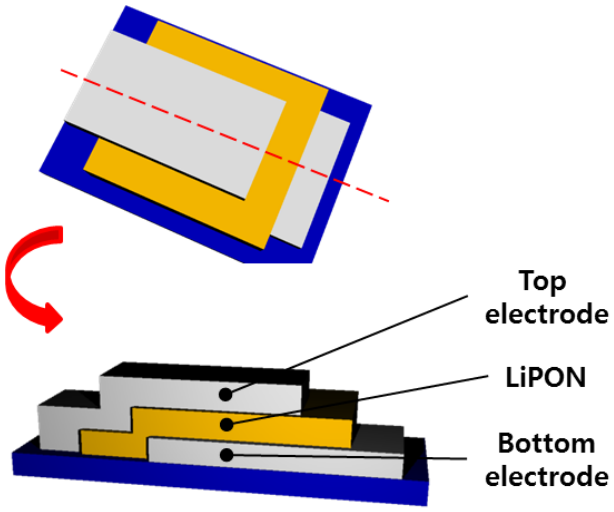

Fig. 3.5 Schematic diagram of electrode/LiPON/electrode sandwich structure

Chapter 4 Results and discussion

4.1 Characterization of LiPON electrolyte

The 2 inch $LiPO_4$ target was prepared for RF sputtering, and sputtering process was operated in N_2 atmosphere. As shown in Fig 4.1, the cross-sectional SEM images indicate the deposition rate of LiPON was kept constant at 2.83 nm/min and show smooth and dense thin film without any cracks and pores.

X-ray diffraction patterns of LiPON thin film is shown in Fig. 4.2, and the film did not exhibit any peaks except the peaks of substrate because of its amorphous nature. In case of LiPON thin film, the amorphous state is advantageous for batteries because the ionic conductivity is generally better than the crystalline films.

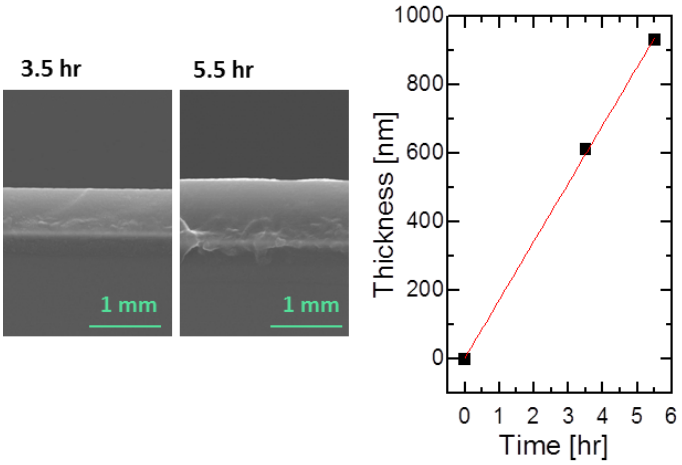

Fig 4.1 SEM images of LiPON film on Si substrate and the graph of deposition rate

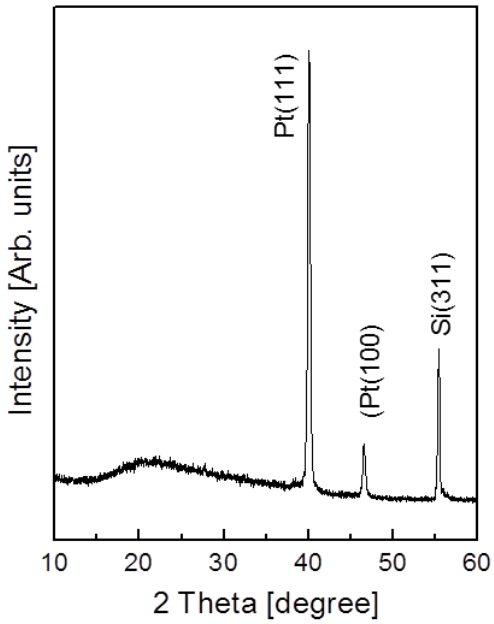

Fig. 4.2 XRD pattern of as-deposited LiPON thin film

Fig. 4.3 shows the auger electron spectroscopy depth profile of LiPON film. The atom contents in the film including Li, N, P, and O were not change with the depth. The data indicates the nitrogen in the film was uniformly incorporated, and this incorporation in the film increased ionic conductivity. This is because the electronegativity of nitrogen is smaller than oxygen, and it caused reduction of the electrostatic attraction to lithium ions.

Lithium ion conductivity of LiPON thin film was measured using impedance measurement in frequencies range of 100 Hz to 100 MHz at room temperature, and impedance diagram of LiPON thin film is shown in Fig.4.4. The ionic conductivity was calculated from the equation of $\sigma = d / (R \times A)$, where d is the thickness of LiPON film, A is the area of the metal electrode and R is the film resistance. The calculated ionic conductivity value was 1.005×10^{-6} S/cm which was typically known.

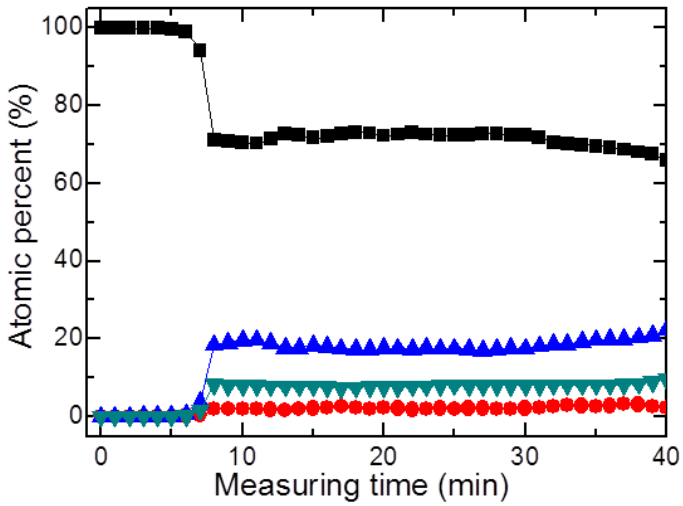

Fig. 4.3 Auger electron spectroscopy depth profile of LiPON film

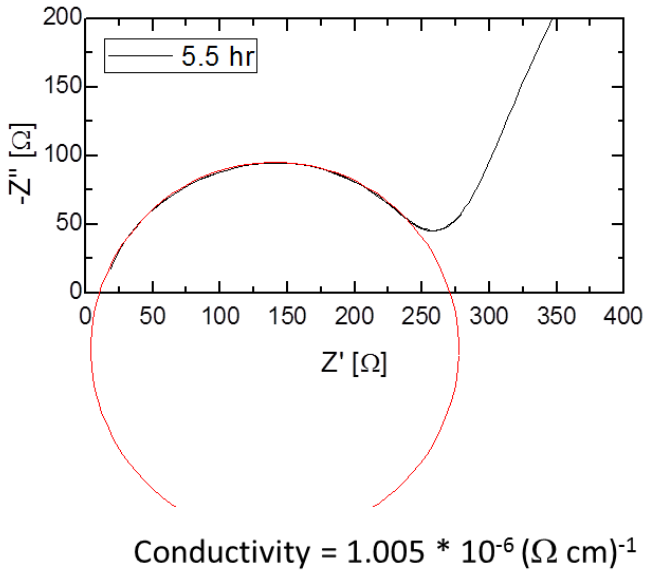

Fig. 4.4 Impedance spectra of LiPON thin film from Pt/LiPON/Pt sandwich structure

4.2 Characterization of $LiNi_{0.5}Mn_{1.5}O_4$ cathode thin film

4.2.1 Structural characteristics

The 280 nm amorphous $LiNi_{0.5}Mn_{1.5}O_4$ cathode thin films were deposited by RF magnetron sputter on the $Pt/Ti/SiO_2/Si$ substrate in order to obtain SEM images and XRD patterns which are shown in Fig 4.5 and Fig.4.6.

The 2 inch $LiNi_{0.5}Mn_{1.5}O_4$ target was prepared for RF sputtering, and sputtering process was operated in Ar and O_2 atmosphere. As shown in Fig 4.5, the cross-sectional SEM images indicate the deposition rate of $LiNi_{0.5}Mn_{1.5}O_4$ cathode thin film was kept constant at 2.3 nm/min and show dense thin film without any pores.

In order to confirm the effect of laser energy, the excimer laser annealing was carried out with the irradiated laser energy of 1000 pulses from 40 mJ/cm^2 to 80 mJ/cm^2. The (111) peak, which is the main peak of spinel phase, is slightly appeared at the 40 mJ/cm^2 and the other peaks of spinel phase such as (311) and (400) are appeared above the laser energy of 70 mJ/cm^2.

Plain-view SEM images of annealed cathode thin films are shown in Fig. 4.7. According to the plain-view images, grain size and morphology of thin films were maintained after laser annealing.

Excimer laser irradiation is instantly transformed into local heat in extremely short time and increase local temperature in the oxide thin film. During this process, the interface between thin film and substrate is damaged if the irradiation energy is too high. As shown Fig 4.7, the melting parts were appeared above laser energy of 80 mJ/cm^2, and the thin film was peeled off from the substrate at laser energy of 90 mJ/cm^2. Therefore, the laser energy was controlled under 90 mJ/cm^2.

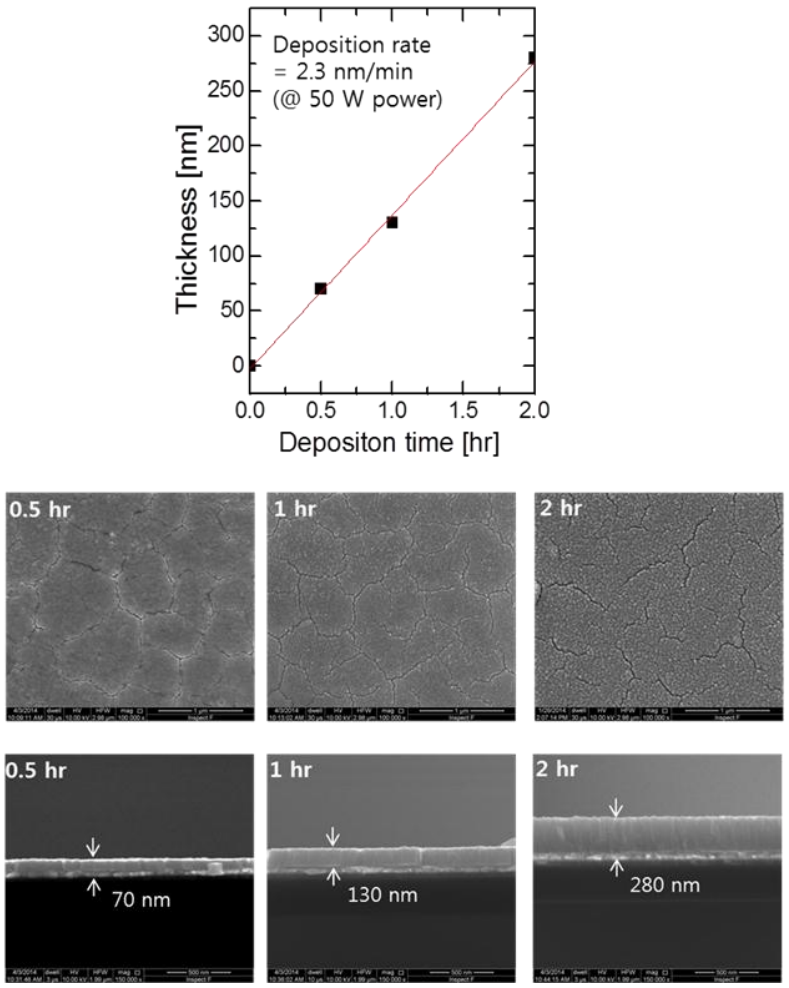

Fig 4.5 cross-sectional SEM images of $LiNi_{0.5}Mn_{1.5}O_4$ cathode thin films deposited with different deposition time

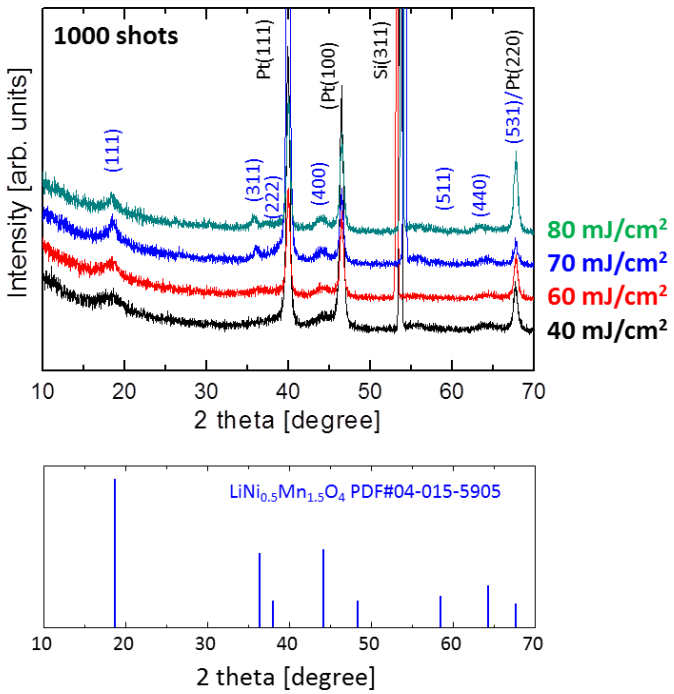

Fig. 4.6 X-ray diffraction spectra of laser-annealed $LiNi_{0.5}Mn_{1.5}O_4$ cathode thin film at various laser energies with 1000 shots

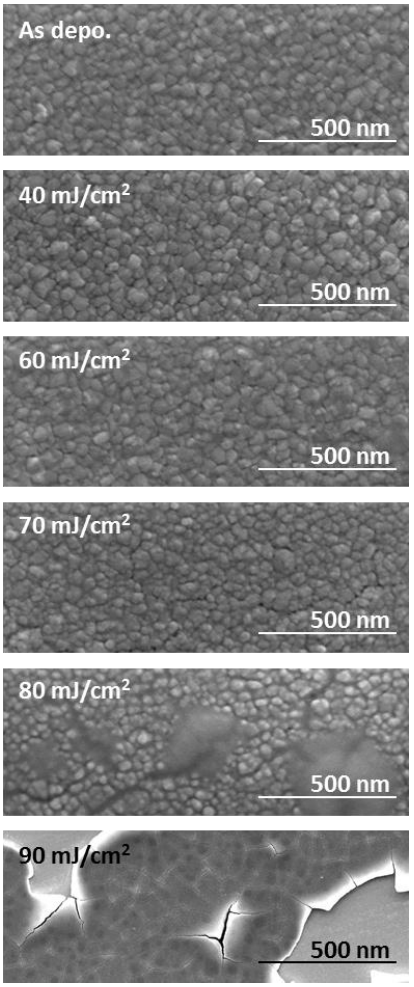

Fig. 4.7 plain-view SEM images of the $LiNi_{0.5}Mn_{1.5}O_4$ thin films annealed with the irradiated laser energy of 1000 pulses from 40 mJ/cm^2 to 90 mJ/cm^2

Fig. 4.8 shows XRD patterns and plain-view SEM images of the $LiNi_{0.5}Mn_{1.5}O_4$ cathode thin films annealed at excimer laser energy of 70 mJ/cm^2 with different shot number. As observed earlier, there is no any peak appeared in the XRD pattern. However, the single $LiNi_{0.5}Mn_{1.5}O_4$ spinel phase formed without a second phase after irradiation above 500 shots. The morphology of thin films is not affected by shot number of irradiation. Dense film without pore and crack were obtained. From XRD and SEM data, the shot number was controlled above 500 shots.

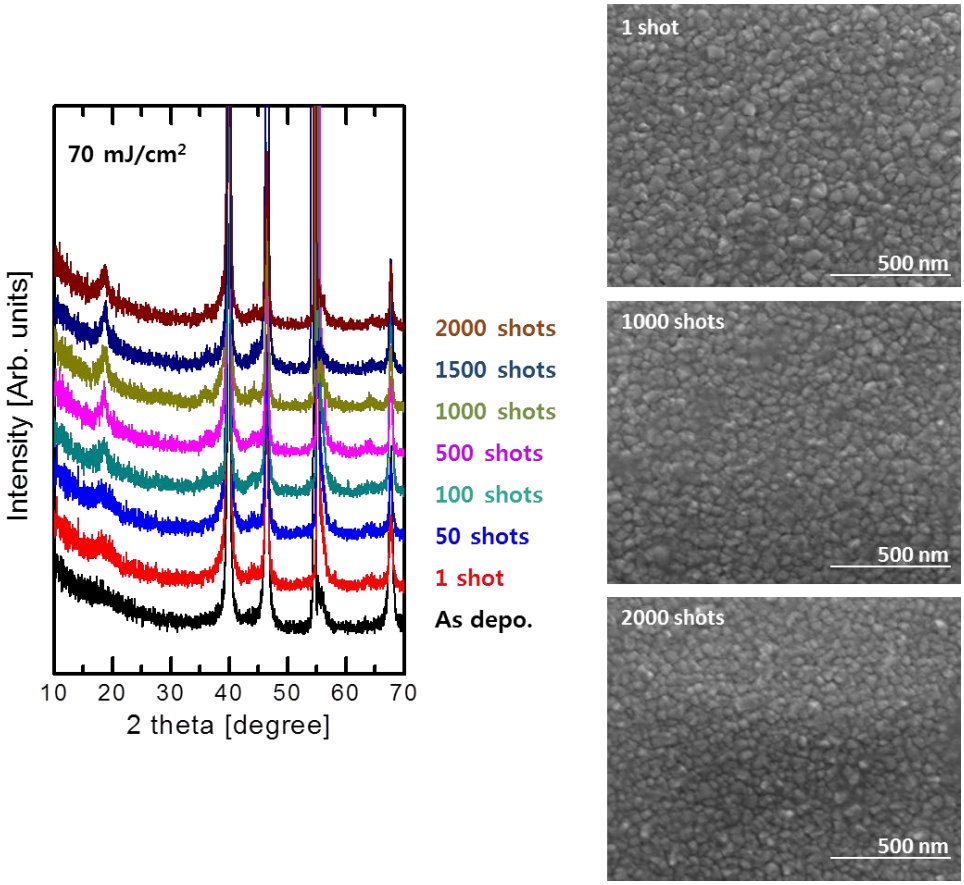

Fig. 4.8 X-ray diffraction spectra and plain-view SEM images of laser-annealed $LiNi_{0.5}Mn_{1.5}O_4$ cathode thin film at various shots number at 70 mJ/cm^2

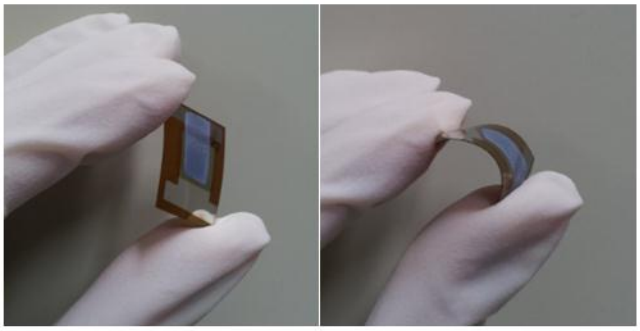

Fig. 4.9 photographic image of flexible thin film batteries

4.3 $LiNi_{0.5}Mn_{1.5}O_4$/LiPON/Li flexible thin film batteries

After investigating the structural properties, the electrochemical behavior of each sample was examined. The electrochemical properties of $LiNi_{0.5}Mn_{1.5}O_4$/LiPON/Li structure flexible thin film batteries on polyimide substrate, as a function of laser energy, are shown in Fig. 4.10. The initial voltage profiles and differential capacity curves were obtained with different laser energy at 0.4 C-rate. Well-defined redox peaks of $Ni^{2+/4+}$ are observed around 4.6 V at laser energy of 70 mJ/cm^2, but weak redox peaks are observed at 4.1 V which is attributed to the redox reaction of $Mn^{3+/4+}$.

Also, Fig. 4.11 shows discharge capacity profile of 3 types of thin film batteries cycled at different current rate which is 0.4 and 0.2 C-rate in voltage range of 3.4 to 4.9 V. At 0.4 C, the electrode achieved a first discharge capacity of 9.47, 11.61, 12.63 μAh/μm-cm^2 with excimer laser energy of 60, 70, 80 mJ/cm^2, respectively. After 5 cycles, the electrode achieved a discharge capacity of 8.24, 11.10, 11.94 μAh/μm-cm^2 with excimer laser energy of 60, 70, 80 mJ/cm^2, respectively. From these data, the capacity retention is calculated as 87.01, 95.58, 94.60 percent with excimer laser energy of 60, 70, 80 mJ/cm^2. As the current rate decreased from 0.4 to 0.2 C, the discharge

capacity increased; the initial capacity and 20th cycled capacity of 60 mJ/cm^2 annealed sample is 16.13 and 13.51 μAh/μm-cm^2; the initial capacity and 20th cycled capacity of 70 mJ/cm^2 annealed sample is 19.71 and 16.04 μAh/μm-cm^2; the initial capacity and 20th cycled capacity of 80 mJ/cm^2 annealed sample is 20.90 and 14.60 μAh/μm-cm^2. The capacity retention is calculated as 83.76, 81.39, 69.85 percent with excimer laser energy of 60, 70, 80 mJ/cm^2, respectively. The initial capacity of 70 mJ/cm^2 annealed sample is slightly lower than 80 mJ/cm^2 annealed samples, but capacity retention shows much better value. Therefore, laser energy of 70 mJ/cm^2 seems a better option for annealing $LiNi_{0.5}Mn_{1.5}O_4$ cathode thin film.

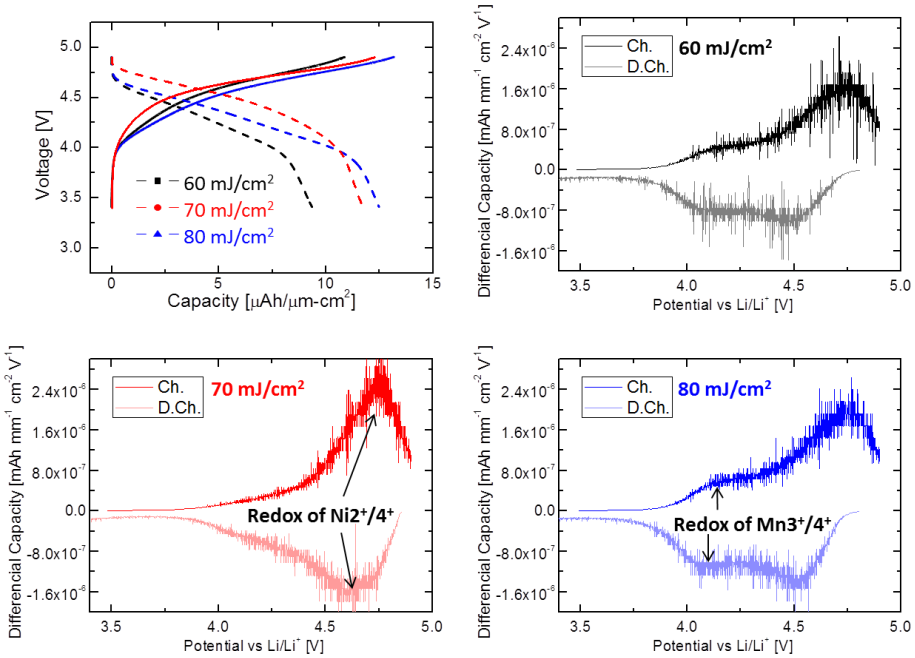

Fig. 4.10 first-cycle voltage profile and differential capacity plots of $LiNi_{0.5}Mn_{1.5}O_4$/LiPON/Li structure flexible thin film batteries, as a function of laser energy. Cycling took place between 3.4 V and 4.9 V at a cycling rate of 25.8 μAh/cm^2 (0.4 C)

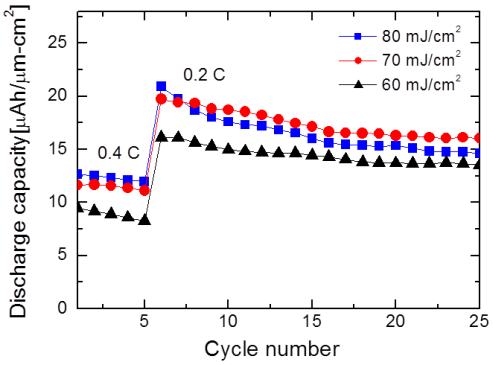

	0.4 C-rate			0.2 C-rate		
	Initial capacity [μAh/μm-cm²]	**Last capacity** [μAh/μm-cm²]	**Retention** [%]	**Initial capacity** [μAh/μm-cm²]	**Last capacity** [μAh/μm-cm²]	**Retention** [%]
60 mJ/cm²	9.46949	8.24023	87.01	16.13394	13.51406	83.76
70 mJ/cm²	11.61453	11.10105	95.58	**19.70674**	**16.03874**	**81.39**
80 mJ/cm²	12.62653	11.94505	94.60	20.89895	14.59726	69.85

Fig. 4.11 plain-

In order to confirm the effect of laser shot number, the irradiation was carried out at 500, 1000, and 2000 shots of laser with the energy of 70 mJ/cm^2. The discharge profiles of $LiNi_{0.5}Mn_{1.5}O_4$/LiPON/Li structure flexible thin film batteries on polyimide substrate, as a function of laser pulse number, are shown in Fig. 4.12. The batteries are cycled between 3.4 V and 4.9 V at cycling rate of 0.1, 0.2, and 0.4 C. The first discharge capacity of 500, 1000, and 2000 shots at 0.1 C was 12.87, 26.38, and 16.40 μAh/μm-cm^2, respectively. Therefore, 1000 shots annealed at laser energy of 70 mJ/cm^2 sample seems a better option for annealing $LiNi_{0.5}Mn_{1.5}O_4$ cathode thin film.

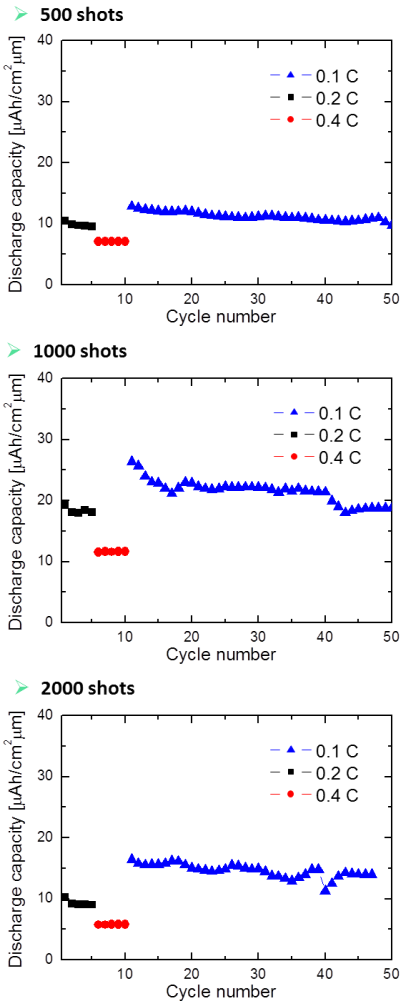

Fig. 4.12 rate capability for the $LiNi_{0.5}Mn_{1.5}O_4$/LiPON/Li structure flexible thin film batteries. The cells were cycled between 3.4 and 4.9 V with various rates.

Fig. 4.13 demonstrates bending testing at various radius conditions from 3 mm to 9 mm. SEM images were employed to observe the morphology and adhesion of the thin films after bending testing compared with nonbending status. There is no discernible cracking, exfoliation, or other change in microstructure. When looking at the interface between electrode and current collector, there is no delamination or cracking even bending radius is over 9 mm.

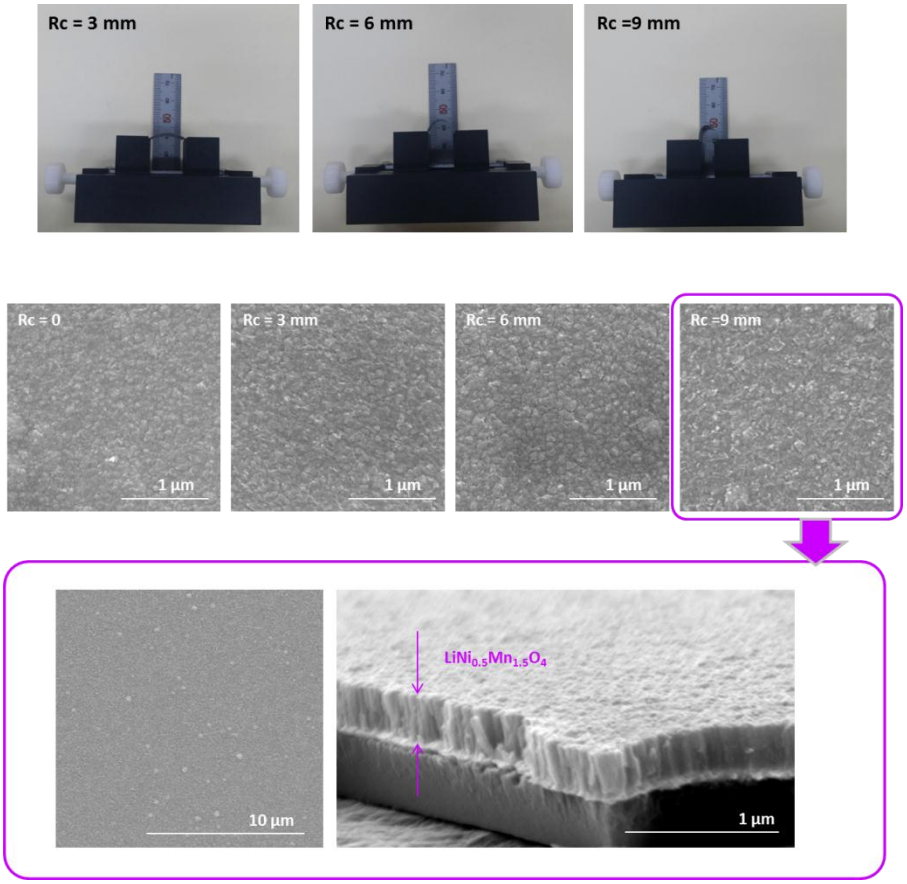

Fig. 4.13 photograph of the robustness tests of flexible thin film batteries on a bending stage machine at bending radius of 3 mm, 6 mm, and 9mm. Plain-view and cross-sectional SEM images of flexible thin film batteries after 10 cycles bending tests at various bending radius.

Chapter 5 Conclusions

In conclusion, we have successfully obtained excimer laser annealed $LiNi_{0.5}Mn_{1.5}O_4$ cathode thin films on polyimide substrate. Structural and electrochemical characteristics of excimer laser annealed thin films were investigated as a function of irradiated laser energy and shot number. The higher energy density than 80 mJ/cm^2 caused crack, exfoliation and defect in the $LiNi_{0.5}Mn_{1.5}O_4$ films, and the electrochemical properties of 1000 shots irradiated film shows the best performance. By using $LiNi_{0.5}Mn_{1.5}O_4$ cathode thin film annealed by optimized condition, we can simply fabricate all-solid-state flexible thin film batteries exhibiting great capacity and cycling stability. Not only is the fabrication process uncomplicated, but it also can be applied on any type of substrates because the laser can selectively anneal $LiNi_{0.5}Mn_{1.5}O_4$ thin film without thermal damage of substrate. The batteries is capable of above 4 V charge/discharge voltage and initial capacity of 26.38 μAh/μm-cm^2. Also, thin films are well maintained under mechanical bending. Therefore, these batteries make it possible to be applied in flexible electronic devices, bendable micro

energy storage system, implantable medical devices, and micro-robot vehicles.

References

1. G. H. Gelinck, H. E. A. Huitema, E. Van Veenendaal, E. Cantatore, L. Schrijnemakers, J. B. P. H. Van der Putten, T. C. T. Geuns, M. Beenhakkers, J. B. Giesbers, B. H. Huisman, E. J. Meijer, E. M. Benito, F. J. Touwslager, A. W. Marsman, B. J. E. Van Rens, and D. M. De Leeuw, "Flexible active-matrix displays and shift registers based on solution-processed organic transistors," *Nat Mater,* 3[2] 106-10 (2004).
2. S. Kim, Y. Hwang, T. H. Kwon, J. Lee, I. K. Lim, S. K. Park, Y. K. Kim, H. Kim, and S. J. Kang, "Safety and Performance Evaluation Methods for Implantable Cardioverter Defibrillator," *2013 International Conference on Ict Convergence (Ictc 2013): Future Creative Convergence Technologies for New Ict Ecosystems* 383-83 (2013).
3. S. J. Kim and J. S. Lee, "Flexible Organic Transistor Memory Devices," *Nano Lett,* 10[8] 2884-90 (2010).
4. L. J. Guo, X. L. Pan, Q. Li, F. Zheng, and Z. Bao, "A Survey on the Gastrointestinal Capsule Micro-Robot Based on Wireless and Optoelectronic Technology," *J Nanoelectron Optoe,* 7[2] 123-27 (2012).
5. G. Anthes, "Technology Skin-like Electronic Patch Unveiled," *Commun Acm,* 54[10] 14-14 (2011).
6. Y. H. Kwon, S. W. Woo, H. R. Jung, H. K. Yu, K. Kim, B. H. Oh, S. Ahn, S. Y. Lee, S. W. Song, J. Cho, H. C. Shin, and J. Y. Kim, "Cable-Type Flexible Lithium Ion Battery Based on Hollow Multi-Helix Electrodes," *Adv Mater,* 24[38] 5192-97 (2012).
7. M. Koo, K. I. Park, S. H. Lee, M. Suh, D. Y. Jeon, J. W. Choi, K. Kang, and

K. J. Lee, "Bendable Inorganic Thin-Film Battery for Fully Flexible Electronic Systems," *Nano Lett,* 12[9] 4810-16 (2012).

8. E. Quartarone and P. Mustarelli, "Electrolytes for solid-state lithium rechargeable batteries: recent advances and perspectives," *Chem Soc Rev,* 40[5] 2525-40 (2011).
9. A. Ueda, M. Nagao, A. Inoue, A. Hayashi, Y. Seino, T. Ota, and M. Tatsumisago, "Electrochemical performance of all-solid-state lithium batteries with Sn4P3 negative electrode," *J Power Sources,* 244 597-600 (2013).
10. H. Kitaura, A. Hayashi, T. Ohtomo, S. Hama, and M. Tatsumisago, "Fabrication of electrode-electrolyte interfaces in all-solid-state rechargeable lithium batteries by using a supercooled liquid state of the glassy electrolytes," *J Mater Chem,* 21[1] 118-24 (2011).
11. J. F. M. Oudenhoven, L. Baggetto, and P. H. L. Notten, "All-Solid-State Lithium-Ion Microbatteries: A Review of Various Three-Dimensional Concepts," *Adv Energy Mater,* 1[1] 10-33 (2011).
12. K. R. Ragavendran, L. Lu, B. J. Hwang, K. Barner, and A. Veluchamy, "Trap State Spectroscopy of LiMyMn2-yO4 (M = Mn, Ni, Co): Guiding Principles for Electrochemical Performance," *J Phys Chem C,* 117[8] 3812-17 (2013).
13. A. Pecora, L. Maiolo, M. Cuscuna, D. Simeone, A. Minotti, L. Mariucci, and G. Fortunato, "Low-temperature polysilicon thin film transistors on polyimide substrates for electronics on plastic," *Solid State Electron,* 52[3] 348-52 (2008).
14. W. Chung, M. O. Thompson, P. Wickboldt, D. Toet, and P. G. Carey, "Room temperature indium tin oxide by XeCl excimer laser annealing for flexible display," *Thin Solid Films,* 460[1-2] 291-94 (2004).

국문초록

최근 스마트 카드, 바이오 센서, 롤-업 디스플레이 등 다양한 종류의 플렉서블 전자 제품의 발전에 따라 그의 동력원으로 사용되는 플렉서블 특성을 갖는 리튬박막전지의 개발이 요구되고 있다. 가볍고 저가의 플렉서블 박막전지를 구현하기 위해서는 폴리머 기판을 사용하는 것이 필수적이다. 하지만, 박막전지의 중요한 구성요소인 양극 박막의 결정화를 위하여 고온에서의 열처리 공정이 필요하게 되는데 이러한 공정의 결과로 낮은 열 저항성을 갖는 폴리머 기판이 손상되어 박막전지의 구현이 어렵게 된다. 따라서 저온에서 양극을 결정화 시킬 수 있는 새로운 공정이 요구된다.

본 연구에서는 $LiNi_{0.5}Mn_{1.5}O_4$ 양극 박막, LiPON 전해질 박막, Li 음극 박막을 이용하여 폴리이미드 기판위에 플렉서블 전 고상 박막전지를 구현하였다. 이 때 비정질 상태로 증착된 $LiNi_{0.5}Mn_{1.5}O_4$ 양극 박막은 엑시머 레이저 어닐링 방법을 통하여 저온에서 결정화 되었다. 조사 된 엑시머 레이저는 양극 박막이 흡수하여 선택적으로 결정화 시키기 때문에 기판의 손상없이 박막전지를 구현할 수 있었다. 양극 박막의 결정성 및 표면 구조를 확인하기 위하여 X-선 회절 분석 및

전자주사현미경 분석이 사용되었으며 70 mJ/cm^2의 레이저 에너지로 1000회 조사 한 경우 가장 우수한 결정성을 나타내었다. 이러한 결과를 토대로 플렉서블 전 고상 박막전지를 제작 하였으며 이러한 전지는 우수한 전기화학 성능(초기 용량 26.38 μAh/μm-cm^2, 4 V 이상의 출력 전압)을 보여주었다. 따라서 엑시머 레이저 어닐링을 이용하여 폴리머 기판 위에 제작한 플렉서블 전 고상 박막전지는 차후 플렉서블 전자 소자의 에너지원으로 사용될 수 있을 것으로 기대된다.

주요어 : 플렉서블 리튬 박막 전지, $LiNi_{0.5}Mn_{1.5}O_4$, 엑시머 레이저 어닐링, 스퍼터링

학 번 : 2012-22575